The Condition of Failure for Sands

La Condition de Rupture des Sables

by W. M. KIRKPATRICK, B.Sc., Ph.D., A.R.T.C., Department of Civil and Mechanical Engineering, Royal College of Science and Technology, Glasgow, Scotland

Summary

This paper describes an investigation into the conditions of failure for drained tests on sands. The shape of the experimental surface of failure, in a principal stress coordinate system, is found. This experimental surface is compared with the surfaces representing existing theories or adaptations to existing theories in order that the best failure theory for the material can be chosen.

Points at different positions on the failure surface are obtained from the results of triaxial compression and axial extension tests together with the results from tests performed on a new apparatus called the thick cylinder apparatus. The design and description of the thick cylinder apparatus are given. The results show good agreement with the Mohr–Coulomb theory and it is concluded that the Mohr–Coulomb theory provides a reliable means of predicting failure in sands under conditions of full drainage.

Sommaire

Dans cet article l'auteur examine les conditions de rupture dans des essais drainés effectués sur des sables. On trouve ainsi, dans un système de coordonnées des contrainte principale, la forme de la surface expérimentale. On compare la surface expérimentale aux surfaces représentant les théories actuelles ou les adaptations de ces dernières pour permettre de choisir la meilleure théorie de rupture pour le matériau en question.

On obtient les points qui se trouvent en différents endroits sur la surface à partir de résultats d'essais basés sur une compression triaxiale et sur un allongement axial, ces résultats étant combinés avec ceux obtenus au cours des essais effectués avec un nouvel appareil appelé appareil à cylindre épais. L'étude et la description de ce dernier sont présentées dans ce rapport.

Les résultats obtenus s'accordent bien avec la théorie de Mohr–Coulomb et on en tire la conclusion que la théorie de Mohr–Coulomb fournit un moyen sûr pour prédire la rupture dans les sables soumis à des conditions de drainage complet.

Introduction

In dealing with three-dimensional stress systems it is convenient to visualize a state of stress, in terms of its three principal stresses, as the rectangular coordinates of a point in space. If all the stress combinations sufficient to cause failure are represented in this way they would trace out a surface in space called the surface of failure. The object of the experimental work described in this paper is to establish the shape of the surface of failure for sand.

The Mohr–Coulomb Failure Surface

The Coulomb equation for the failure of soils can be stated

$$S = C + \sigma \tan \phi \qquad \ldots\ (1)$$

This equation represents a special case of the Mohr theory of strength where in the Mohr envelope is a straight line inclined to the normal stress axis at angle ϕ. The use of the Coulomb equation to represent the Mohr envelope in the Mohr diagram is termed the Mohr–Coulomb theory of strength in this paper.

In terms of the principal stresses the Mohr–Coulomb condition for a sand can be expressed

$$\sigma_3/\sigma_1 = \lambda \qquad \ldots\ (2)$$

where

$$\lambda = \frac{1 - \sin\phi}{1 + \sin\phi}$$

Assuming an isotropic material, the condition can be put in its most general form as

$$\{(\sigma_1 - \sigma_2)^2 - [\sin\phi(\sigma_1 + \sigma_2)]^2\}\{(\sigma_2 - \sigma_3)^2 - [\sin\phi(\sigma_2 + \sigma_3)]^2\}$$
$$\{(\sigma_3 - \sigma_1)^2 - [\sin\phi(\sigma_3 + \sigma_1)]^2\} = 0 \qquad \ldots\ (3)$$

representing six flow conditions from which the intermediate principal stress is always absent.

The shape of the surface of failure, in a three-dimensional system of coordinates (σ_1, σ_2, σ_3), that equation 3 represents, can best be seen from the diagrams of Fig. 1. With the coordinate directions as shown in Fig. 1a (compressive stress $+_{ve.}$) a section of the surface formed by a plane containing both the σ_2 axis and the space diagonal will appear as in Fig. 1b. A view of a right section of the surface, i.e. a section taken at right angles to the space diagonal, will be as shown in Fig. 1c*.

The shape of the right section is a hexagon with sides of equal length but opposite sides not being parallel. The surface in space is a hexagonal pyramid with its apex at the origin of the system of coordinates and extending in the compressive directions of the axes. The right sections are similar in shape but increase in dimension with the distance along the space diagonal at which they are taken.

Application of Other Possible Theories

The shape of the experimental surface of failure may conform to that of the Mohr–Coulomb theory or it may diverge greatly from it. To have any practical value however it must be readily expressed mathematically. Existing information on the behaviour of sands under stress comes mainly from the results of the triaxial compression test. It is usual to assume the Mohr–Coulomb theory in the interpretation of these results. Other failure criteria could be suggested, however, which in the light of existing experimental knowledge would be just as satisfactory. In this respect the possibility is considered of the Von Mises and the Tresca (NADAI, 1950) theories of strength being made to suit sands by extending the conditions of failure to include dependency on the mean normal stress. The theory which provides the surface which conforms closest to the experimental surface will be chosen to represent the failure conditions for the sand.

The extended Von Mises condition becomes

$$(\sigma_1 - \sigma_2)^2 + (\sigma_2 - \sigma_3)^2 + (\sigma_3 - \sigma_1)^2 = [K_1 \tfrac{1}{3}(\sigma_1 + \sigma_2 + \sigma_3)]^2 \qquad \ldots\ (4)$$

where K_1 is a constant related to $f(\sin\phi)$.

* Due to lack of space a detailed derivation of the shape of the failure surface cannot be given here. The reader seeking further information is referred to KIRKPATRICK (1954).

This is a particular case of a more general extension to the Von Mises condition suggested by SCHLEICHER (1925). The surface represented by equation 4 is a cone with its apex at the origin and its axis lying along the space diagonal. Right sections of the surface are circles (Fig. 1d) and can be made to coincide with the Mohr–Coulomb surface along the major principal stress directions at A, B and C.

The extended Tresca condition is expressed by

$$\{(\sigma_1 - \sigma_2)^2 - [K_2\tfrac{1}{3}(\sigma_1 + \sigma_2 + \sigma_3)]^2\}$$
$$\{(\sigma_2 - \sigma_3)^2 - [K_2\tfrac{1}{3}(\sigma_1 + \sigma_2 + \sigma_3)]^2\}$$
$$\{(\sigma_3 - \sigma_1)^2 - [K_2\tfrac{1}{3}(\sigma_1 + \sigma_2 + \sigma_3)]^2\} = 0 \quad \ldots . \quad (5)$$

where K_2 is a constant also related to $f(\sin\phi)$.

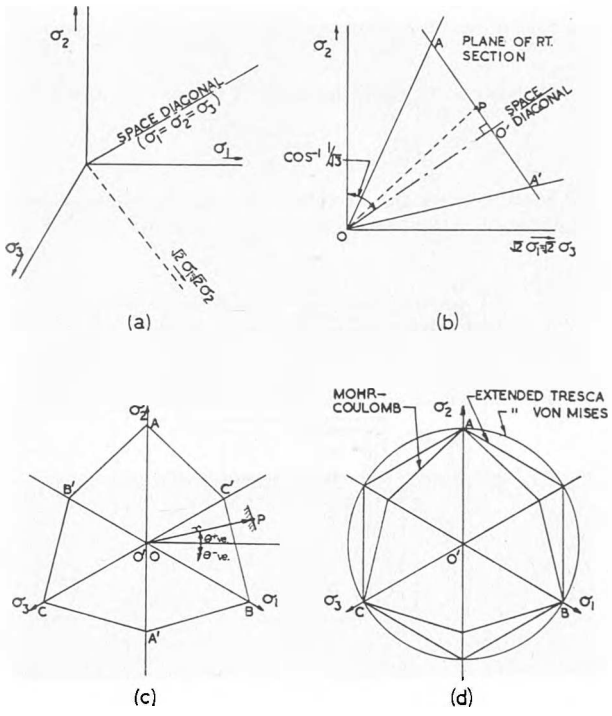

Fig. 1 (a) The coordinate directions
Les axes des coordonnées
(b) Section of Mohr–Coulomb surface made by plane containing σ_2 and space diagonal
Coupe de la surface de Mohr–Coulomb effectuée au moyen du plan contenant σ_2 et diagonale spatiale
(c) Right section of Mohr–Coulomb surface
Coupe droite de la surface de Mohr–Coulomb
(d) Right sections of Mohr–Coulomb, extended Tresca and extended Von Mises surfaces
Coupes droites de Mohr–Coulomb, surfaces prolongées de Tresca ainsi que celles de Von Mises

The surface represented by equation 5 is a hexagonal pyramid and, as in the above case, has its apex at the origin and its axis along the space diagonal. Right sections of the surface are regular hexagons (Fig. 1d) and can be made to coincide with the Mohr–Coulomb surface at A, B and C.

Method of Illustrating the Experimental Right Section

In the determination of the surface of failure for an isotropic material a 60 degree sector of the right section need only be considered since the surface in other sectors will be similar to or mirror images of this. Such a 60 degree sector is $BO'C'$ in Fig. 1c and the problem is to obtain experimental points between C' and B to establish the shape. If a point P (coordinates $\sigma_1, \sigma_2, \sigma_3$) lies on the experimental surface in this sector its position on the right section can be defined by its cylindrical coordinates $r = O'P$ and θ. It is known, however, that the shape of the surface in space is such that the size of the right sections will vary depending on the distance along the space diagonal at which they are taken. Consequently, to establish the shape of the right section from individual test results the points on the failure surface that these results represent must all lie on the same right section. The condition for this to occur is that for each result $\sigma_1 + \sigma_2 + \sigma_3 =$ constant. It is impractical to arrange this condition experimentally but if it can be proved that the generating curves bounding the surface in space e.g. OA, OC' and OP (Fig. 1b and c) are straight lines the difficulty of illustrating the right section can be overcome. The results later show that these lines are straight and the right section is illustrated by plotting the tangent of the angle at the origin subtended by $O'P$, i.e. $\tan < POO'$ instead of the true distance $O'P$. The right section obtained in this way is called the reduced right section. The cylindrical coordinates of P in sector $C'O'B$ are then

$$O'P = \tan\left[\cos^{-1}\left(\frac{1}{\sqrt{3}} \cdot \frac{\sigma_1 + \sigma_2 + \sigma_3}{\{\sigma_1^2 + \sigma_2^2 + \sigma_3^2\}^{\frac{1}{2}}}\right)\right]$$

$$\theta = -\tan^{-1}\left[\frac{1}{\sqrt{3}} \cdot \frac{2\sigma_2 - \sigma_3 - \sigma_1}{\sigma_3 - \sigma_1}\right]$$

θ varies between + 30 and − 30 degrees measured from OX in the directions shown in Fig. 1c ($\theta = -\tan^{-1} 1/\sqrt{3}u$ where u is the well known parameter introduced by LODE, 1926).

Stress Systems Required

To find the shape of the right section of the failure surface experimental points are required:

(1) Along direction $O'B$, Figs. 1c and d; where $\sigma_1 > \sigma_2 = \sigma_3$ and $\theta = -30$ degrees.

(2) Along $O'C'$ which gives the greatest difference between the Mohr–Coulomb and the other theories; here $\sigma_1 = \sigma_2 > \sigma_3$; $\theta = +30$ degrees.

(3) On the surface between B and C' to establish the shape between 1 and 2; here $\sigma_1 > \sigma_2 > \sigma_3$ and θ varies between − 30 and + 30 degrees.

The shape of the surface in space must also be investigated. The above points are thus required on right sections at varying distances from the origin.

Experimental Work

Tests on the triaxial apparatus—The first stress system in the previous paragraph is that obtaining in the standard triaxial compression test. Tests were conducted under constant confining pressures, failure being caused by an increasing axial stress.

The stress system $\sigma_1 = \sigma_2 > \sigma_3$ was also obtained in the triaxial apparatus. In this case the axial stress was reduced until failure occurred. The confining pressure was kept constant during the test. Similar tests to these have been previously reported by BISHOP and ELDIN (1953) and HABIB (1952 and 1953) and are referred to as 'axial extension tests'. For a detailed description of the axial extension tests used in this investigation the reader is referred to KIRKPATRICK (1954).

For the compression tests the confining pressures were applied through a constant head mercury tank giving a maximum pressure of 70 lb./sq. in. A closed circuit system was introduced for the extension tests increasing the range to 150 lb./sq. in.

Area corrections were applied in the calculation of stresses in the triaxial tests. In the axial extension tests an additional

allowance was made for tensions set up in the rubber membranes.

Complete drainage was allowed in all the tests.

Tests on the Thick Cylinder Apparatus

Design of the apparatus—The method adopted to obtain the variation of σ_2 between the values of σ_1 and σ_3 was to test the soil in the form of thick-walled cylinders. The thick cylinder sample can be constrained by both a bore and an outside pressure, the bore pressure being increased until failure is induced. An element of material is thus subjected to radial, tangential and axial compressive stresses of differing amounts. The axial stress can be varied by applying external loads to the sample.

In the development stages the apparatus was made without the external loading device. The dimensions of the sample were arranged so that the differences of bore and outside pressures acting on the sealed end of the sample would bring the axial stress to a value approximately mid-way between the values of the tangential and radial stresses. It was intended to introduce a loading system similar to that used in the triaxial apparatus at a later stage. The results obtained in tests on sands however were so conclusive that the adaptation for axial loading was not made to the apparatus for this series of tests.

For guidance in the design of the apparatus it was assumed that the Mohr–Coulomb theory of strength is applicable.

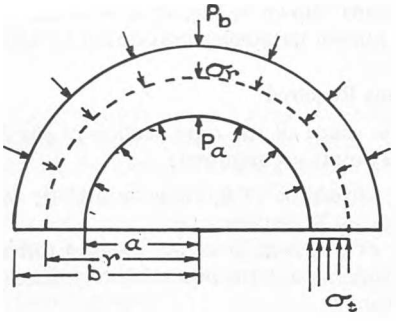

Fig. 2 Stresses in wall of thick cylinder sample
Les efforts dans la paroi de l'éprouvette en forme de cylindre épais

The stresses in a vertical section of the thick cylinder sample are shown in Fig. 2; where b denotes the outside radius, a denotes the bore radius, P_b denotes the outside pressure, P_a denotes the bore pressure, σ_r denotes the radial stress at any radius r, and σ_t denotes the tangential stress at any radius r. Since the forces must be in equilibrium

$$P_a a - \sigma_r r + \int_a^r \sigma_t dr = 0 \qquad \ldots\ (6)$$

σ_r is the major principal stress and σ_t is the minor principal stress. The axial stress is the intermediate principal stress caused by load differences on the sealed end of the sample.

On differentiating (NADAI, 1950), and substituting $\sigma_t = \lambda\sigma_r$ (equation 2), we have at the point of failure

$$\frac{dr}{r} = \frac{d\sigma_r}{\sigma_r(\lambda - 1)} \qquad \ldots\ (7)$$

which on integration becomes

$$\sigma_r = Ar^{(\lambda-1)} \qquad \ldots\ (8)$$

During tests the outside pressure is kept constant and the bore pressure is increased to failure.

Hence at $r = b$, $\sigma_r = P_b$.

Substituting this in 8

$$\sigma_r = P_b\left(\frac{r}{b}\right)^{(\lambda-1)} \qquad \ldots\ (9)$$

giving σ_r and hence σ_t, at any radius r, at failure. The bore pressure sufficient to cause failure will be

$$\sigma_{r,\,(r=a)} = P_a = P_b\left(\frac{a}{b}\right)^{(\lambda-1)} \qquad \ldots\ (10)$$

the corresponding tangential stress at $r = a$

$$\sigma_{t,\,(r=a)} = \lambda P_b\left(\frac{a}{b}\right)^{(\lambda-1)} \qquad \ldots\ (11)$$

The average radial stress in the wall of the sample is

$$\sigma_{r,\,(av.)} = \frac{P_b}{\lambda}\left[\frac{b^\lambda - a^\lambda}{(b-a)b^{(\lambda-1)}}\right] \qquad \ldots\ (12)$$

the average tangential stress from conditions of equilibrium of the sample is

$$\sigma_{t,\,(av.)} = \frac{P_b b - P_a a}{b - a} \qquad \ldots\ (13)$$

the axial stress is constant throughout the sample and is

$$\sigma_{ax.} = \frac{P_b b^2 - P_a a^2}{b^2 - a^2} \qquad \ldots\ (14)$$

The axial stress varies in value between the radial stress and the tangential stress depending on λ and the ratio b/a. A minimum wall thickness of $\frac{3}{4}$ in. was decided upon and for convenience the sample dimensions were fixed at $a = 1\frac{1}{4}$ in., $b = 2$ in., making $b/a = 1{\cdot}6$.

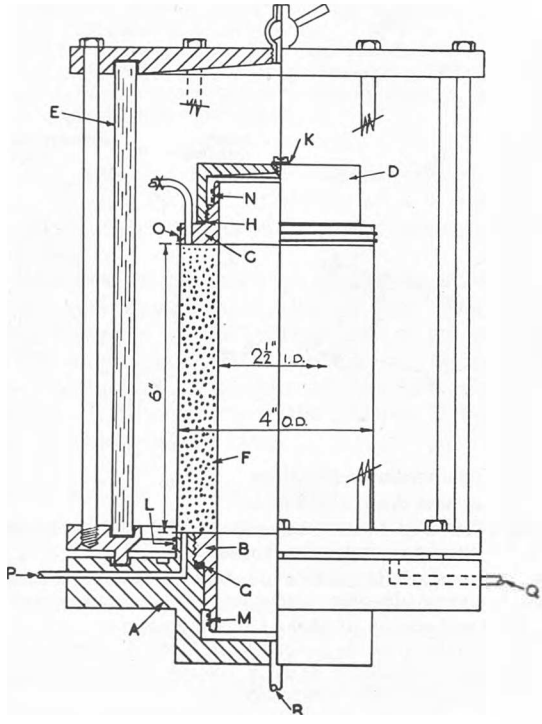

Fig. 3 Thick cylinder apparatus—pressure cell
L'appareil à cylindre épais—cellule de pression

Table 1, which gives the values of $\sigma_r(av.)$, $\sigma_t(av.)$ and $\sigma_{ax.}$ for values of $\lambda = 0{\cdot}3$ and $0{\cdot}2$, shows that the axial stress remains approximately mid-way between the values of the radial and tangential stresses for a wide range of λ.

Description of thick cylinder apparatus and test—A half section of the pressure cell of the thick cylinder apparatus is shown in Fig. 3. The cell parts consist of the base A, the base adaptor B, the sample end-piece C, the sealing cap D and the transparent pressure cylinder E. The sample F is $2\frac{1}{2}$ in. I.D., 4 in. O.D. and approximately 6 in. high.

Table 1

λ	$\sigma_1(\sigma_r av.)$	$\sigma_3(\sigma_t\ av.)$	$\sigma_2(\sigma_{ax.})$	$\frac{\sigma_1+\sigma_3}{2}$
0·3	$1{\cdot}155P_o$	$0{\cdot}347P_o$	$0{\cdot}750P_o$	$0{\cdot}751P_o$
0·2	$1{\cdot}200P_o$	$0{\cdot}240P_o$	$0{\cdot}705P_o$	$0{\cdot}720P_o$

The construction of the apparatus was governed mainly by the necessity to have a complete pressure seal between the bore and the outside of the sample. For this purpose there are gasket seals at G in the base, H on the sample end-piece and K on the sealing cap. The wall thickness of the sample is equal to the combined thicknesses of the raised ring L on the base

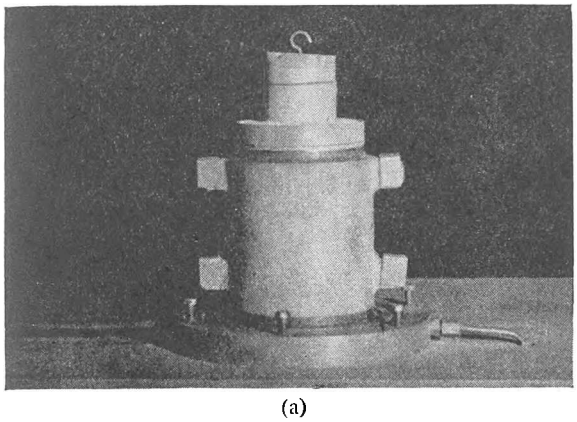

(a)

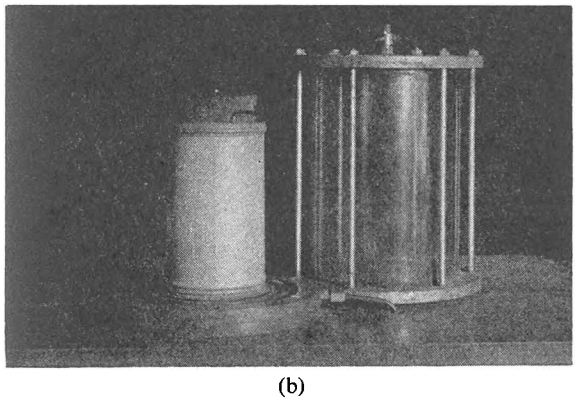

(b)

Fig. 4 (a) Thick cylinder sample under preparation
L'éprouvette du cylindre épais en préparation
(b) Thick cylinder sample ready for test
L'éprouvette du cylindre épais prête pour l'èssai

and the upper threaded portion of the base adaptor B. The base adaptor is made removable to allow the sealing of the inner rubber membrane at M. Other seals are provided at N for the inner membrane and at L and O for the outer membrane.

Sand samples are filled between a central cylindrical wooden former and an outer former consisting of a split steel ring (Fig. 4a). The cap D is screwed down to the sample end-piece after a slight vacuum has been applied to the sample through P. A holding tool which fits into recesses in the sample end-piece is used to prevent torque being applied to the sample during this operation. The outlet K in the cap was introduced to allow the air to be expelled from the bore while filling with water. The transparent outer cylinder E is held to the base by 6 studs. Fig. 4b shows a thick cylinder sample ready to be tested.

The outside pressures are supplied to entry Q from a constant head mercury tank. The bore pressures (to entry R) are applied by a foot controlled pump. The required accuracy in the pressure measurement was obtained by means of a mercury manometer. The use of a narrow gauge tubing for the manometer afforded a degree of strain control in the application of the bore pressures.

A series of thick cylinder tests were performed at outside pressures varying from 14 to 55 lb./sq. in. During the tests the outside pressure was kept constant and failure was induced by increasing the bore pressure. Full drainage was allowed in the tests.

Except when it was desired to study failure types, the tests were stopped as soon as the failure pressure had been reached.

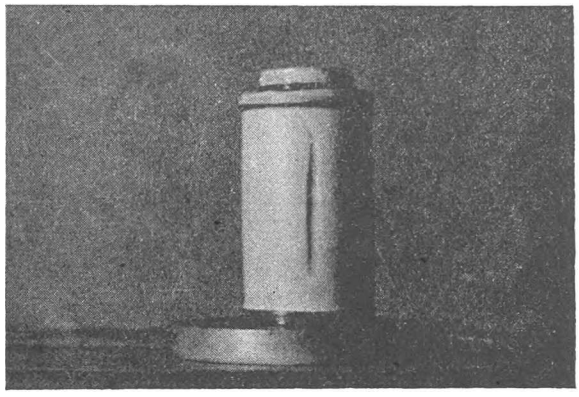

(a)

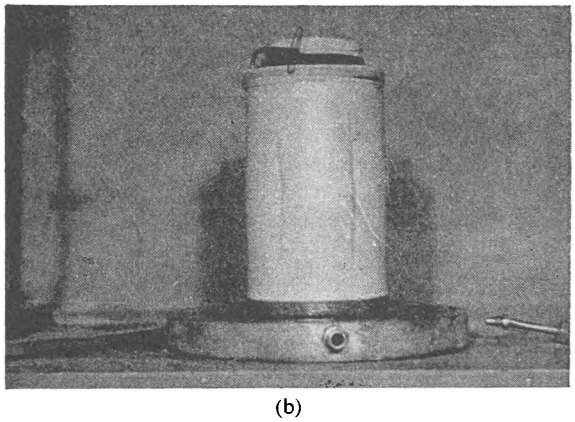

(b)

Fig. 5 (a) Thick cylinder sample with single failure crack
L'éprouvette du cylindre épais avec une seule cassure de rupture
(b) Thick cylinder sample with dual failure cracks
L'éprouvette du cylindre épais avec deux cassures de rupture

The sample was then measured and these measurements used in the stress calculations. Allowance was made for the radial stresses set up in the rubber membranes due to the slight bulging of the sample. The necessary adjustments which had to be made to the measured pressures were small, however, and had a slight effect only at low pressures.

Fig. 5 (a and b) shows thick cylinder samples after failure. Failure in these two samples was taken further than was normal for the tests. The majority of samples failed due to the development of a single vertical crack in the wall, Fig. 5a. In isolated cases dual cracks such as shown in Fig. 5b were obtained. From observation it appeared that the failure crack was formed by slip occurring along a shear trajectory in the wall of the sample.

A more detailed description of the apparatus and the test procedure is given by KIRKPATRICK (1954).

Loch Aline Sand

The sand used in all tests was a medium fine sand obtained from Loch Aline, Scotland: the particles were almost entirely of pure quartz. The grading curve for the sand is shown in Fig. 6. Particles finer than B.S. sieve No. 200 were removed from the natural sand for the convenience of testing.

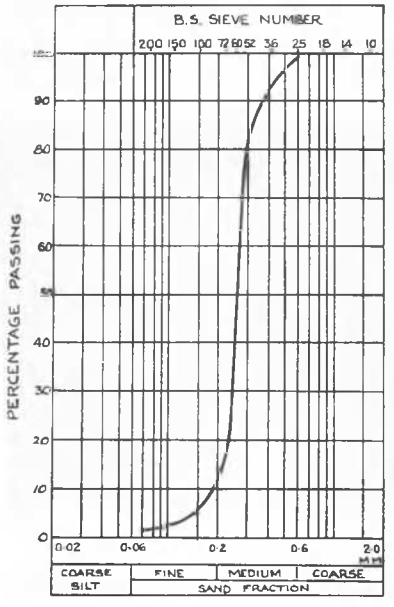

Fig. 6 Grading curve for Loch Aline sand
Courbe granulométrique du sable du Loch Aline

The Filling of Samples

A series of triaxial compression, axial extension and thick cylinder tests were performed. It was desired to fill the samples at minimum porosity to make it simpler for the same densities to be reproduced from sample to sample and in the two different sample forms: this was required so that the Mohr envelopes could be drawn for the tests performed on the triaxial apparatus and so that the results of all three types of test could be inter-related. The low porosities were achieved in the triaxial samples by filling in thin layers and tamping each layer lightly with a $\frac{1}{2}$ in. diameter wooden rod. Corresponding porosities were produced in the thick cylinder samples by vibration on the bore and outside formers during filling. The porosity varied slightly but not significantly from sample to sample. The average porosity for tests performed in the triaxial apparatus was 35·1 per cent and that for the thick cylinder tests was 35·6 per cent. These figures were considered close enough to allow a valid comparison of the results to be made.

Results

In this paper the term point of failure is taken to represent the peak point on the stress-strain curve. The failure stresses are therefore those existing at the peak point.

Triaxial compression and axial extension results—The major stress circles for the compression and axial extension tests are shown in Fig. 7. The positions of the points on the reduced right section, Fig. 8, that these results represent are at 1 for the compression tests and at 2 for the extension tests. The right sections of the theoretical Mohr–Coulomb and the extended Tresca and Von Mises surfaces based on the triaxial compression results are also shown in Fig. 8.

For the range of pressures used it can be said that (1) the Mohr envelopes are straight and pass through the origin of the Mohr diagram; (2) the angle ϕ found in the compression tests is in close agreement with that obtained in the extension tests; and (3) the Mohr–Coulomb theory predicts accurately the

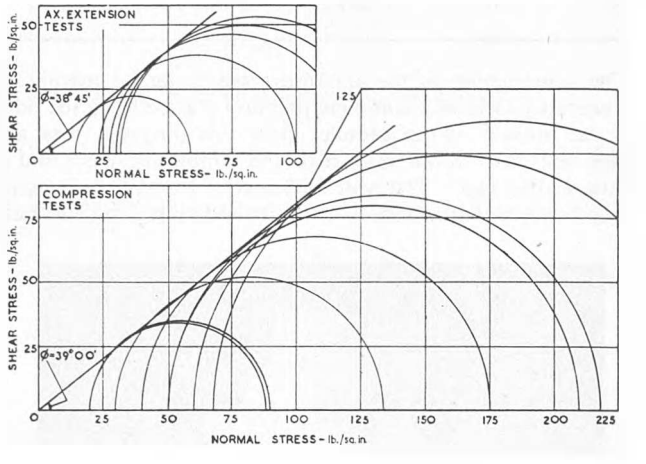

Fig. 7 Mohr diagrams for compression and axial extension tests
Diagrammes de Mohr pour les essais de compression et d'allongement axial

failure conditions for stress systems where $\sigma_1 > \sigma_2 = \sigma_3$ and $\sigma_1 = \sigma_2 > \sigma_3$.

The extended Tresca and Von Mises theories do not fit the results for these stress systems.

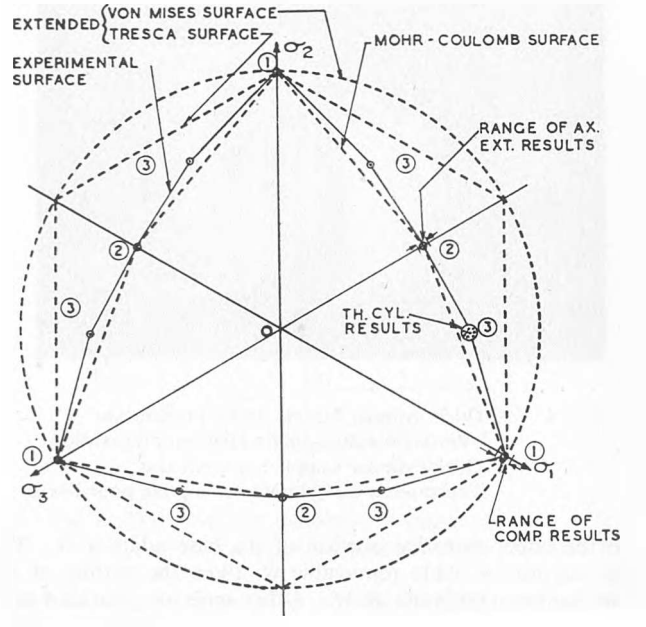

Fig. 8 Reduced right section of experimental surface of failure (average stresses in thick cylinder tests) with theoretical right sections
Coupe droite à échelle réduite de la surface expérimentale de rupture (contraintes moyennes dans les essais au cylindre épais)

Thick cylinder results—In the thick cylinder sample the radial stress at the bore and at the outside are known at failure. The distribution of radial stress through the wall of the sample, however, is not known. In the preliminary analysis of the results a linear distribution of radial stress was assumed, giving

an approximation to the average radial stress at the point of failure. Using this, together with the average tangential stress (equation 13), an approximation to the shape of the experimental right section along directions 3 is obtained (Fig. 8). Although this is an approximation to the right section along directions 3 it shows that the thick cylinder results lie close to the Mohr–Coulomb theory and that the other two theories are again not applicable.

Assuming, as the above illustration shows, that the Mohr–Coulomb theory holds for the material, the distribution of tangential stress can be found and the shape of the failure surface can be checked from the measured radial and axial stresses at the bore and the outside of the sample. The tangential stress $\sigma_t = \lambda\sigma_r$ (equation 2) at any point at failure λ is calculated from equation 10. The stresses obtained in the above manner are shown in Table 2.

Table 2

Test	λ	*At outside*		*At bore*		
		$P_o = \sigma_1$ lb./sq. in.	$\lambda P_o = \sigma_3$ lb./sq. in.	$P_i = \sigma_1$ lb./sq. in.	$\lambda P_i = \sigma_3$ lb./sq. in.	$\sigma_{ax.} = \sigma_2$ lb./sq. in.
1	0·196	14·40	2·82	21·21	4·16	10·50
2	0·208	18·70	3·89	27·18	5·65	13·30
3	0·216	30·60	6·61	44·08	9·52	22·30
4	0·215	38·50	8·28	55·68	11·95	27·95
5	0·192	45·80	8·80	65·75	12·61	32·30
6	0·198	47·92	9·48	68·63	13·60	34·05
7	0·215	50·30	10·81	72·88	15·63	35·90
8	0·219	54·02	11·83	77·16	16·90	38·90
9	0·197	54·80	10·80	78·43	15·40	38·20

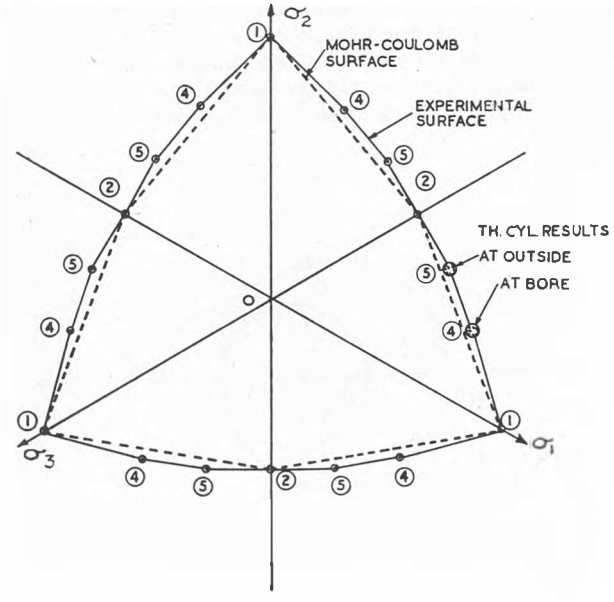

Fig. 9 Reduced right section of experimental surface of failure (stresses at bore and outside in thick cylinder tests)
Coupe droite à échelle réduite de la surface expérimentale de rupture (les efforts aux parois internes et externes dans les essais au cylindre épais)

The reduced right section produced by these results is shown in Fig. 9. The bore stresses are represented at position 4 and the stresses at the outside at position 5. The positions 1 and 2 represent the triaxial compression and axial extension tests as before.

The results lie close to the theoretical Mohr–Coulomb surface based on the results of the triaxial compression tests. They show an increase in strength over that predicted by the theory but the difference is small amounting to approximately 2 degrees in the angle of internal friction. Due to the closeness of the results to the Mohr–Coulomb theory it was considered unnecessary to investigate the failure surface at points intermediate to those already described.

The shape of the experimental right section has been established. It is also necessary, however, to investigate the shape of the surface in space. The fact that the Mohr envelopes, Fig. 7, are straight indicates that the generating lines OA, OA', OB, OB', etc. (Fig. 1) are also straight. Due to the scatter of the results no single generating line contains all the points either for the bore or for the outside in the thick cylinder tests. The points are grouped closely together, however, and an indication that the slopes of the generators along the directions 04 and 05 (Fig. 9) are constant is given in Fig. 10 where the angles made by the lines joining the points on the surface to the origin

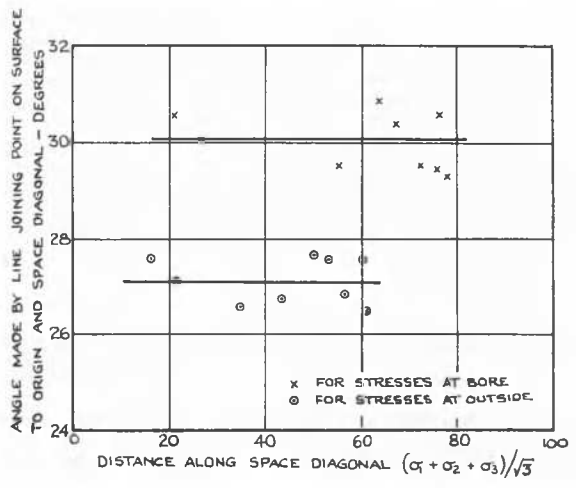

Fig. 10

and the space diagonal (i.e. $< POO'$ Fig. 1) are shown plotted against their distance along the space diagonal.

It can therefore be said that the shape of the surface in space is a straight sided pyramid as predicted by the Mohr–Coulomb theory.

Conclusions

The results show that the Mohr–Coulomb theory provides a reliable means of predicting failure for sands under conditions of complete drainage. For stress systems where $\sigma_2 \fallingdotseq (\sigma_1 + \sigma_3)/2$, obtained in the thick cylinder tests, the theory under-estimates the strength. The under-estimation, however, is considered slight and to have no practical importance. It is thought that the condition of plain strain which approximately obtains in the thick cylinder test may in some way be responsible for the divergence and that the general condition of failure for sands depends to some extent on strain.

The close agreement between the angles of internal friction found in the compression and extension tests was also obtained by Bishop and Eldin (1953). Habib (1952, 1953), however, found the angle obtained in the extension test as much as 7 degrees lower than in the compression test. In view of this conflicting evidence the author performed a further series of extension and compression tests on Loch Aline sand. Close agreement was found in the values of ϕ for the two tests and the agreement was obtained at porosities varying throughout the range for the sand.

The divergence from the theory obtained by Habib in his torsion tests was also large. It is felt however that in these tests a satisfactory method of estimating the effect of the rubber membrane was not found. The torsional resistance of the membrane, which is at the maximum radius of the sample, must be considerable and unless its effect can be estimated precisely little faith can be placed in the results of such tests.

The thick cylinder method of testing was found to be a convenient way of obtaining the required stress systems. The apparatus itself is simple in its operation and is suitable for similar investigations in other types of soil.

The work was carried out during the period 1951–1954 in the Soil Mechanics Laboratory of the Royal Technical College, Glasgow. Thanks are due to Dr W. Frazer, under whose direction the work was conducted, and to Professor A. S. T. Thomson, for permission to use the Laboratory.

References

BISHOP, A. W. and ELDIN, A. K. GAMAL (1953). The effect of stress history on the relation between ϕ and porosity in sand. *Proc. 3rd International Conference on Soil Mechanics and Foundation Engineering*, Vol. 1, p. 100

HABIB, P. (1952). La résistance au cisaillement des sols. *Doctor's Thesis, University of Paris*

— (1953). Influence de la variation de la contrainte principale moyenne sur la résistance au cisaillement des sols. *Proc. 3rd International Conference Soil Mechanics and Foundation Engineering*, Vol. 1, p. 131

KIRKPATRICK, W. M. (1954). The behaviour of sands under three-dimensional stress systems. *Ph.D. Thesis, University of Glasgow*

LODE, W. (1926). Versuche über den Einflus der Mittleren Hauptspannung auf des Fliesen der Metalle Eisen, Kupfer und Nickel. *Zeits. für Physik*, **36**, 913

NADAI, A. (1950). *Theory of Flow and Fracture of Solids*, Vol. 1, Chap. 15, New York; McGraw-Hill

SCHLEICHER, F. (1925). Die Energiegrenze der Elastizität (Plastizitätsbedingung). *Zeits. für ang. Math. Mech.*, **5**, 478